Check for updates

Quantum information processing and quantum optics with circuit quantum electrodynamics

Alexandre Blais [1,2,3 ✉], Steven M. Girvin [4,5] and William D. Oliver[6,7,8]

Since the first observation of coherent quantum behaviour in a superconducting qubit, now more than 20 years ago, there have been substantial developments in the field of superconducting quantum circuits. One such advance is the introduction of the concepts of cavity quantum electrodynamics (QED) to superconducting circuits, to yield what is now known as circuit QED. This approach realizes in a single architecture the essential requirements for quantum computation, and has already been used to run simple quantum algorithms and to operate tens of superconducting qubits simultaneously. For these reasons, circuit QED is one of the leading architectures for quantum computation. In parallel to these advances towards quantum information processing, circuit QED offers new opportunities for the exploration of the rich physics of quantum optics in novel parameter regimes in which strongly nonlinear effects are readily visible at the level of individual microwave photons. We review circuit QED in the context of quantum information processing and quantum optics, and discuss some of the challenges on the road towards scalable quantum computation.

avity quantum electrodynamics (QED) studies the interaction of light and matter at its most fundamental level: the coherent interaction of single atoms with single photons. Over the past 40 years, this exploration has led to advances in experimental techniques to the level where control of the quantum state of single atoms is now possible, developments that have provided exquisitely precise tools to probe the counterintuitive nature of quantum physics[1,2]. To reach a regime where coherent light–matter coupling overwhelms all decay rates, such that quantum effects become important, cavity QED relies on atoms with a large atomic electric dipole moment and cavities that confine the electromagnetic field in a small region of space.

However, quantum coherence is not limited to natural atoms, and the first conclusive signatures of a coherent superposition of two states in an engineered quantum system were observed two decades ago via the atomic physics techniques of Rabi oscillations[3] and Ramsey interference fringes[4,5]. At the heart of such experiments is a Josephson junction-based device acting as a single artificial atom[6]. However, unlike natural atoms, superconducting artificial atoms must be somewhat coerced into behaving quantum mechanically with appropriate design and operation at cryogenic temperatures. Nevertheless, formidable progress in this direction has been made over the past 20 years, and by some measures, artificial atoms are now on par with or even surpassing their natural counterparts. In addition, superconducting quantum circuits can be strongly and controllably coupled to electromagnetic fields confined in circuit elements such as inductors and capacitors. In other words, the physics of cavity QED can naturally be explored in circuits, an observation that has opened the field of circuit QED[7–9]. Beyond quantum optics, circuit QED achieves in a single architecture the essential requirements for universal quantum computing and is now a leading architecture for the realization of a scalable quantum computer[10].

This Review surveys how the degree of control and connectivity of artificial atoms enabled by circuit QED can be exploited both to explore the physics of cavity QED and quantum optics on a chip, as well as to build promising quantum technologies. We first

introduce the basic concepts of circuit QED and how the new parameter regimes that can be obtained in circuit QED, compared with cavity QED, lead to new possibilities for quantum optics. Next, we discuss circuit QED in the context of quantum information processing. We then present perspectives on the next steps for the field of circuit QED towards quantum computation, first with quantum error correction (QEC) and then by discussing some of the challenges associated with scaling to larger systems.

Circuit QED in a nutshell
In this section, we summarize the basic theory of circuit QED.

Superconducting quantum circuits. The basic ingredients of circuit QED are illustrated in Fig. 1. They consist of a superconducting qubit (green) embedded in a high-quality microwave oscillator (blue), such as a superconducting coplanar-transmission-line resonator, a lumped-element inductor–capacitor (LC) circuit, or a three-dimensional (3D) cavity. When working with a transmission-line resonator (Fig. 1a), the qubit is fabricated in close proximity to the centre conductor of the resonator[7]. This centre conductor is interrupted by gaps leading to capacitive coupling to the input and output ports of the resonator (grey in Fig. 1a). At these points, the current vanishes and these open boundary conditions result in normal modes with well-separated frequencies[11]. By working with centimetre-long resonators, the fundamental frequency is in the microwave regime and is typically chosen to be between 5 and 15 GHz. These frequencies are high enough to avoid thermal photon population at the temperature where these devices are operated (~10 mK), but still in a convenient range for microwave control electronics. Moreover, dissipation is minimized by fabricating the circuits using aluminium, which is superconducting below 1 K. The distribution of the electric field for the second mode of the resonator is illustrated by the orange lines in Fig. 1a.

Close to one of the mode frequencies, the resonator is well approximated by a single parallel LC oscillator where the effective

Fig. 1 | Realizations of circuit QED. a, Schematic representation of a superconducting transmon qubit (green) coupled to a 1D transmission-line resonator. The transmon is formed by two superconducting islands connected by a Josephson junction. With lateral dimensions (~300 μm) much smaller than that of the resonator (~1 cm), multiple transmons can be fabricated in the same resonator (not shown). The input and output ports of the resonator are shown in grey. The orange lines and arrows illustrate the electric field distribution for the resonator's second mode. **b**, Lumped-element version where an LC circuit (blue) plays the role of the oscillator. The voltage source (grey) is used to control the quantum state of the transmon (green). **c**, Three-dimensional coaxial cavity with its electric field distribution (solid orange lines) and evanescent field (dashed orange lines). Panels adapted with permission from: **a**, ref. [7], APS; **c**, ref. [17], APS.

inductance L and capacitance C are chosen to match the mode frequency $\omega_r = 1/\sqrt{LC}$ and the characteristic impedance, $Z_r = \sqrt{L/C}$ (Fig. 1b). In a quantized model, the Hamiltonian of this circuit takes the usual form for a harmonic oscillator

$$\hat{H}_{LC} = \hbar\omega_r \hat{a}^\dagger \hat{a} \qquad (1)$$

The creation operator $\hat{a}^\dagger$ can be expressed as $\hat{a}^\dagger = \sqrt{1/2\hbar Z_r}(\hat{\Phi} - iZ_r\hat{Q})$ where $\hat{\Phi}$ is the flux threading the inductor and $\hat{Q}$ the charge on the capacitor with $[\hat{\Phi}, \hat{Q}] = i\hbar$. The operator $\hat{a}^\dagger$ thus creates a quantized excitation of the oscillator's charge and flux degrees freedom or, equivalently, of its electric and magnetic fields. In short, the action of $\hat{a}^\dagger$ is the creation of a photon of frequency ω_r localized in the LC circuit. It is worth noting that while the average voltage across the LC circuit vanishes in the vacuum state, its root-mean-square value is non-zero: $V_{zpf} = \langle 0|\hat{V}^2|0\rangle^{1/2} = \sqrt{\hbar\omega_r/2C}$, where $\hat{V} = \hat{Q}/C$. Typical circuit parameters result in a $V_{zpf} \approx 1$ μV (ref. [12]). Going back to the transmission-line resonator of Fig. 1a where the separation between the centre conductor and the ground plane is $d \approx 5$ μm, this corresponds to a zero-point electric field as large as $E_{zpf} = V_{zpf}/d \approx 0.2$ V m^{-1} in this region of the circuit. These large quantum fluctuations of the electric field result from the small mode volume of the resonator and are one of the reasons why light–matter coupling can be much larger in circuit QED than in cavity QED. Importantly, the lifetime of single microwave photons in these structures can be long, approaching 0.1 ms in coplanar resonators[13–16] and 1 ms in 3D cavities of the type illustrated in Fig. 1c[17].

The second crucial ingredient is the qubit. There are many types of superconducting qubits, and here we focus on the transmon, which is the simplest and most widely used[18]. As illustrated in Fig. 1, it consists of a capacitively shunted Josephson junction with capacitance C_S. The Josephson junction is a nonlinear and non-dissipative circuit element which, in the transmon, essentially plays the role of a nonlinear inductance causing the energy levels of the circuit to be non-uniformly distributed. This situation is well described at low energies by the Hamiltonian

$$\hat{H}_T = \hbar\omega_q \hat{b}^\dagger \hat{b} + \hbar K \hat{b}^\dagger \hat{b}^\dagger \hat{b}\hat{b} \qquad (2)$$

In this expression, $\hbar\omega_q = \sqrt{8E_C E_J} - E_C$ is the transition frequency between the first two states of the transmon, with $E_C \approx e^2/2C_S$ the charging energy, where e is the elementary charge and E_J the Josephson energy. The second term of $\hat{H}_T$ is a Kerr nonlinearity with negative Kerr constant $\hbar K = -E_C/2$. In other words, the transmon is a weakly nonlinear oscillator with negative anharmonicity $2K/2\pi = -E_C/h \approx 200$ MHz. Importantly, the above expressions are valid in the transmon limit, where the ratio $E_J/E_C \gtrsim 50$ is large. In practice, this ratio is achieved by using a very large shunting capacitance making the transmon a physically large circuit (Fig. 1a).

In contrast to the LC oscillator, the nonlinearity of the transmon makes it possible to address its first two levels with minimal leakage to higher-energy states. In this case, the transmon reduces to an effective two-level system with states labelled $\{|0\rangle, |1\rangle\}$ and which can be used as a qubit for quantum information processing. To manipulate the qubit state, voltage pulses at the 0–1 transition frequency ω_q are sent to the transmon from a capacitively coupled microwave source (Fig. 1b). This coherent microwave drive is represented by an additional term in the transmon Hamiltonian of the form $\hat{H}_{drive} = \epsilon(t)(\hat{b}^\dagger + \hat{b})$ (ref. [19]). By precisely controlling the amplitude, phase and duration of the pulse $\epsilon(t)$, it is possible to prepare arbitrary states of the transmon with gate fidelity as high as 99.95% (ref. [20]).

Owing to its simple design and long coherence time, the transmon qubit is currently the most widely studied. It is, however, only one of several flavours of superconducting qubits. Other contemporary superconducting qubits include the flux qubit[21] with a large shunting capacitance[22], the fluxonium[23] and the recently realized 0–π qubit[24]. The reader interested in learning more about the different types of superconducting qubits can consult recent reviews[25,26].

Light–matter coupling in a circuit. Up to now, we have discussed the oscillator and the transmon qubit individually, but things get much more interesting when these two elements interact. Indeed, just as a microwave source can drive qubit transitions, the zero-point voltage fluctuations V_{zpf} of the capacitively coupled oscillator can stimulate energy exchange between the qubit and the oscillator. To model this situation, the amplitude $\epsilon(t)$ proportional to a classical voltage in $\hat{H}_{drive}$ is replaced by the LC oscillator's voltage operator $\hat{V}$ leading to the qubit–oscillator interaction Hamiltonian

$$\hat{H}_{coupling} = \hbar g(\hat{a}^\dagger + \hat{a})(\hat{b}^\dagger + \hat{b}) \qquad (3)$$

where all the prefactors are packaged in the coupling constant g (refs. [7,18]). Combining with $\hat{H}_{LC}$ and $\hat{H}_T$, this Hamiltonian takes a particularly simple form in the two-level approximation where $\hat{b} \to \hat{\sigma}_-$, with $\hat{\sigma}_-$ the Pauli lowering operator

$$\hat{H}_{JC} = \hbar\omega_r \hat{a}^\dagger \hat{a} + \frac{\hbar\omega_q}{2}\hat{\sigma}_z + \hbar g(\hat{a}^\dagger \hat{\sigma}_- + \hat{a}\hat{\sigma}_+) \qquad (4)$$

In this Hamiltonian, we have also dropped rapidly oscillating terms from $\hat{H}_{coupling}$ that, in the usual parameter range, only lead to a negligibly small frequencies shift[27].

The Hamiltonian $\hat{H}_{JC}$ represents the exchange of a single microwave photon from the LC oscillator to the qubit, and vice versa. It is known as the Jaynes–Cummings Hamiltonian and describes light–matter interaction in cavity QED[1]. Importantly, in circuit QED, this interaction can be made much stronger than is realized in atomic systems[8]. Here, the coupling g can be expressed as the product of the electric dipole moment of the qubit and of the zero-point electric field of the harmonic mode[1,7,28]. As already mentioned, very large quantum fluctuations of the field are obtained by engineering harmonic modes with small mode volumes. Moreover, because the transmon is such a large object (Fig. 1a), its dipole moment is substantially larger than that of, for example, the single Rydberg atoms used in microwave cavity QED. Alternatively, large coupling can also be achieved with large mode volumes, for example, with the 3D coaxial cavity illustrated in Fig. 1c, by compensating the reduction in field amplitude by working with even larger transmon qubits[29].

Quantum optics on a chip

The very strong light–matter coupling that is possible in circuit QED together with the large nonlinearity of Josephson junctions and the flexibility in designing superconducting quantum circuits is opening the possibility to explore the very rich physics of quantum optics on a chip. In this section, we provide a few illustrations of this growing research direction[30]. Because microwaves are the natural frequency range for these circuits, the experiments discussed here are realized with microwave rather than optical photons. With much of the pioneering work in cavity QED also involving microwave photons, this is not unique to circuit QED[1,9].

A distinguishing feature of circuit QED is, however, the strength of light–matter coupling g that can be realized. To play an important role, this quantity should overwhelm the atomic relaxation and dephasing rates, as well as the cavity decay rate. In this situation, atom and photon states hybridize to form entangled states. On resonance, this coherent interaction leads to an avoided crossing of size $2g$ between the atom and the oscillator energy levels, known as the vacuum Rabi splitting. While the first observation in circuit QED[8] of this hallmark signature of the strong coupling regime had a peak separation to linewidth ratio of ~10, on par with atomic systems[31–33], more recent experiments easily display ratios of several hundreds (Fig. 2).

The new parameter regimes that can be achieved in circuit QED have also made it possible to experimentally test long-standing theoretical predictions of quantum optics. One example is the effect of squeezed radiation on atoms. As early as the mid-80s, theorists had predicted how dephasing and resonant fluorescence of an atom would be modified under squeezed radiation[34,35]. Testing these ideas, however, requires solving multiple experimental challenges, such as squeezing all the spatial modes of the field coupled to the atom and minimizing losses[36]. Despite much effort, simultaneously addressing all of these challenges remains difficult in atomic systems[37]. The situation is drastically different in circuit QED where the nonlinearity of Josephson junctions can be exploited to readily produce squeezed radiation[38]. Moreover, this radiation can easily be guided via on- and off-chip transmission lines to a qubit playing the role of an artificial atom. The reduced dimensionality of electrical circuits limits the number of modes involved in atomic interactions, such that squeezing a single mode can have a substantial effect. Taking advantage of this, what would have been a tour de force experiment in atomic systems has been realized in circuit QED, confirming the theoretical predictions[39,40].

In addition, the strong nonlinearity of superconducting qubits has been used to prepare exotic quantum states of the microwave field. The first experiment in this direction took advantage of the possibility to rapidly frequency-tune superconducting qubits to transfer, one by one, qubit excitations to the oscillator[41]. In this way, oscillator Fock states up to $|n = 6\rangle$ have been prepared. Using a
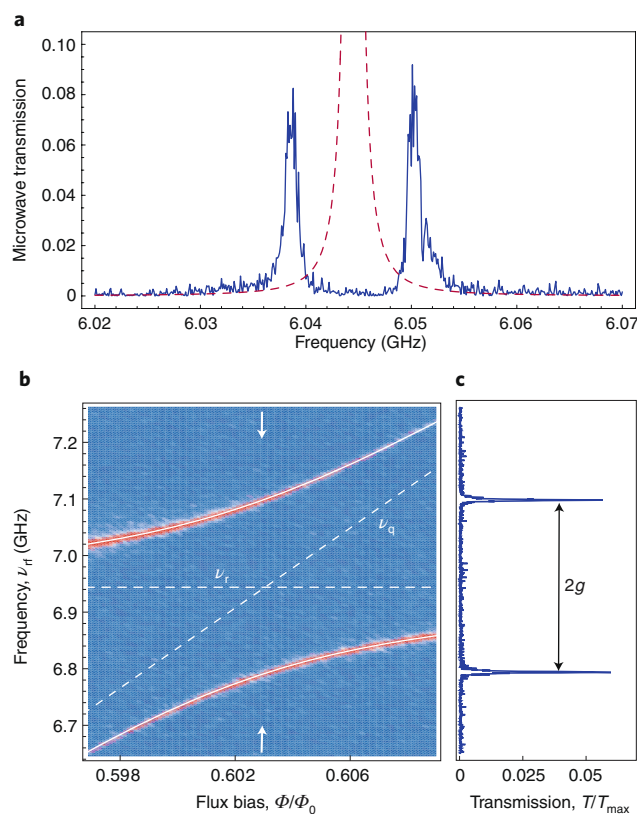
Fig. 2 | Vacuum Rabi splitting. a, Transmission power spectrum of transmission-line resonator as a function of the input drive frequency displaying clear vacuum Rabi splitting. The solid blue line is measured at the qubit-resonator resonance $\Delta = 0$ while the dashed red line shows the spectrum measured at strong detuning $|\Delta| = |\omega_q - \omega_r| \gg g$ where only the resonator is probed. **b**, The resonator transmission spectra versus drive frequency ν_{rf} and external flux bias Φ/Φ_0, where Φ_0 is the flux quantum. The flux bias is used to tune the qubit frequency and allows mapping of the full qubit-resonator anti-crossing. Blue corresponds to low transmission and red to high transmission. The solid white line correspond to the dressed qubit-resonator energies, while the dashed white lines indicate the bare resonator frequency $\nu_r = \omega_r/2\pi$ and qubit transition frequency $\nu_q = \omega_q/2\pi$ with its flux dependence. **c**, Resonator transmission at the flux bias indicated by the arrows in **b** and corresponding to qubit-resonator resonance. The vacuum Rabi splitting is clearly observed. Panels adapted with permission from: **a**, ref. [8], Springer Nature Ltd; **b,c**, ref. [123], Springer Nature Ltd.

similar sequential approach, the same authors have also prepared arbitrary superpositions of the oscillator field and used the qubit to measure the field's Wigner function (something quite challenging to do in ordinary quantum optics) (Fig. 3)[42]. An alternative approach avoiding the long preparation time that is typical of the above sequential method takes advantage of the dispersive regime discussed in the next section to drive qubit transitions conditionally on the Fock state of the cavity[43]. Together with ideas borrowed from optimal control[44], this approach has been used to prepare Fock states up to $|n = 6\rangle$ with high fidelity, as well as the superposition of coherent states known as four-legged cat states[45] and so-called Gottesman–Kitaev–Preskill (GKP) grid states[46]. As will be discussed below, these types of intricate states of the microwave field are a useful resource for QEC.

Quantum information processing

To have long coherence times, qubits must be well decoupled from sources of noise and uncontrollable degrees of freedom, such as
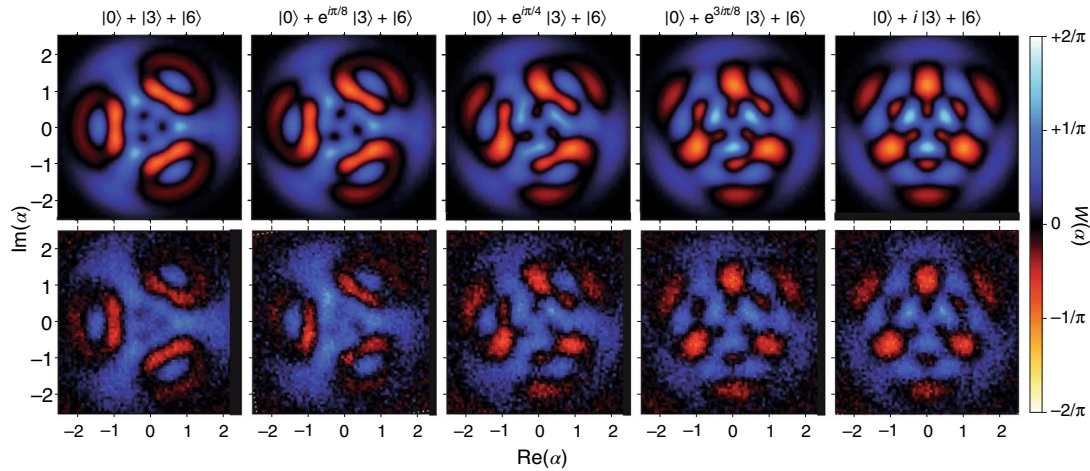
Fig. 3 | Wigner functions $W(\alpha)$ of the microwave fields. Wigner tomography of the Fock state superpositions $|0\rangle + e^{ik\pi/8}|3\rangle + |6\rangle$ for $k = 0$ to 4 as obtained by repeated resonant interactions between a superconducting qubit and a microwave resonator. The top row corresponds to the theoretical prediction and the bottom row corresponds to the experimental data. Figure reproduced with permission from ref. [42], Springer Nature Ltd.

electromagnetic noise, dielectric losses and quasiparticles (broken Cooper pairs). However, qubits must be strongly coupled to external control electronics to realize fast logical operations and readout. Simultaneously satisfying these seemingly contradictory requirements is one of the main challenges in designing and operating qubits. Circuit QED is an appealing approach to solve these challenges in a solid-state system[7,47]. Indeed, the oscillator can be used to measure the qubit state (and vice versa) and can act as a 'quantum bus' mediating interactions between qubits. In this way, it is possible to entangle qubits separated by as much as a centimetre. As we will see below, the oscillator itself can also be the primary holder of the quantum information, with the qubits playing a secondary role as controllers.

In the context of quantum information processing, it is useful to work in the dispersive regime where the detuning between the qubit and the oscillator frequency is made much larger than the light–matter coupling strength, $|\Delta| = |\omega_q - \omega_r| \gg g$. A first advantage of working at large detunings is that the resonator acts as a band-pass filter protecting the qubit from noise at its transition frequency, which is the cause of unwanted qubit transitions (for example, vacuum noise, which causes spontaneous emission of microwave photons when the qubit is in its excited state). A second advantage results from the fact that, in this limit, the Jaynes–Cummings Hamiltonian is well approximated by the simpler effective model[1,7]

$$\hat{H}_{disp} = \hbar(\omega_r + \chi\hat{\sigma}_z)\hat{a}^{\dagger}\hat{a} + \frac{\hbar\omega_q}{2}\hat{\sigma}_z \qquad (5)$$

with $\chi = g^2/\Delta$ known as the dispersive shift. As is made clear by the first term of $\hat{H}_{disp}$, in the dispersive regime, the oscillator frequency is pulled by its interaction with the qubit to a new qubit-state dependent frequency, $\omega_r \pm \chi$. Measuring the response of the oscillator to a probe tone can therefore reveal the state of the qubit[7,48]. Owing to the development of quantum-limited amplifiers[49], this approach is used to realize single-shot qubit readout with fidelity above 99% in under 100 ns measurement time[50]. Moreover, collecting the terms proportional to $\hat{\sigma}_z$ in $\hat{H}_{disp}$ makes it clear that the dispersive coupling also leads to a photon-number-dependent shift of the qubit frequency, $\omega_q + 2\chi\hat{a}^{\dagger}\hat{a}$ (ref. [51]). As a result, by measuring this quantized light shift of the qubit, it is possible to resolve different low photon-number states in the oscillator with very high fidelity (ref. [52]). As alluded to in the previous section, this very large light shift

enables sophisticated quantum control capabilities, something which we come back to below.

By coupling multiple qubits to the same oscillator, the latter can also play the role of a quantum bus mediating entanglement between the qubits[7,47]. The interaction of each qubit with the oscillator takes the form of $\hat{H}_{coupling}$ and multiple approaches have been theoretically proposed and experimentally implemented to turn this qubit-resonator coupling into an effective qubit–qubit interaction[19,25,47]. In the simplest case, two qubits can be brought in resonance with each other while remaining far detuned from the resonator. In this situation, a qubit excitation can be mediated virtually by the resonator, leading to a qubit–qubit exchange interaction of the form $\chi(\hat{\sigma}_{+1}\hat{\sigma}_{-2} + \hat{\sigma}_{-1}\hat{\sigma}_{+2})$ (refs. [47,53]). Maximally entangled states can be generated from this interaction, for example, by tuning the qubits in resonance with each other for a time $t = \pi/4\chi$. Using more sophisticated methods, resonator-mediated two-qubit gates have been experimentally realized with fidelity as high as 99.1% in a gate time of 160 ns (ref. [54]). Alternatively, two-qubit gates can also be mediated by tunable coupling circuit elements reaching fidelities of 99.5% in ~50 ns (refs. [25,55]). While not using a resonator to mediate entanglement, these experiments rely on the dispersive readout to measure the qubit.

Although readout and gate fidelity in circuit QED are now above 99% and several tens of qubits can be operated together to carry non-trivial computing tasks[10], much work remains to be done before large-scale quantum computation can be realized with this architecture. Fortunately, circuit QED offers many advantages when it comes to QEC, a concept that is essential for quantum computation and to which we now turn.

Quantum error correction

The idea that QEC is possible in principle[56–58] is in some ways even more remarkable than the idea of quantum computation itself. Quantum computers are in one sense analogue devices with continuously growing errors. Error correction succeeds because special types of measurements can be constructed that collapse the state to a small number of discrete possibilities, either no error or some specific discrete error on a specific qubit.

Remarkably, this collapse can be arranged to yield information about the error that occurred, but no information about the quantum state, which would lead to destruction of the underlying computation that is in progress. Early experiments using NMR
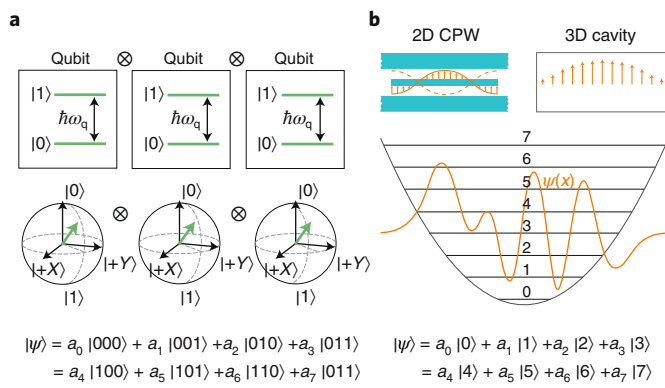
Fig. 4 | QEC hardware. a,b, A Hilbert space of dimension 8 can be constructed either from three discrete-variables (qubits) (**a**) or one continuous-variable system (**b**, top): either a coplanar waveguide (2D CPW) resonator or a 3D cavity microwave resonator and one transmon controller (not shown). The top portion of **a** illustrates the energy spectrum of three separate two-level systems whose individual states can be described by three Bloch spheres (middle portion of panel). Here $|X\rangle$ and $|Y\rangle$ are linear superpositions of the qubit basis states $|0\rangle$ and $|1\rangle$. The bottom portion of **a** gives the most general (possibly entangled) state of the system in the energy eigenbasis of the three qubits. The middle portion of **b** illustrates the quadratic potential energy of the harmonic oscillator mode with its discrete energy levels labelled by photon number. The oscillatory orange curve represents the wave function $\psi(x)$ in the position basis corresponding to a general superposition of states in the photon number (Fock) basis shown in the bottom portion of the panel. The coefficients a_j are exactly the same in both the discrete variable and continuous variable cases and there is a one-to-one correspondence between qubit states and cavity states. For example, qubit state $|101\rangle$ corresponds to photon number state $n = 5$, since the binary representation of 5 is 101.

spectroscopy[59,60], ion traps[61,62], solid-state defect centres[63,64] and superconducting qubits[65,66] demonstrated QEC protocols, but various technical limitations prevented them from successfully extending the lifetime of the quantum information beyond the best value naturally occurring in the systems. Three different circuit QED schemes have recently approached or slightly exceeded this break-even point[46,67,68] using a so-called continuous-variable approach described below.

QEC requires encoding information in a high-dimensional system ('logical qubit') comprising entangled states of multiple 'physical qubits'. The information must be hidden in the non-classical correlations among the physical qubits so that no single physical qubit 'knows' the state of the logical qubit. In this way, the environment cannot damage the information by collapsing the state of one physical qubit (or in the case of codes tolerant to n errors, by collapsing the state of up to n physical qubits). Logical information thus has to be encoded via 'unnatural' high-weight (that is, multi-qubit) entangling operations to be protected from 'natural' errors that are (assumed to be) low weight.

A crucial step is to extract information ('error syndromes') about errors without causing back action on the encoded system. A necessary (but not sufficient) condition to avoid back action is that the measurement yields no information about the logical state, only about the errors. Error syndrome information is stored in unnatural high-weight operators, but can be measured using multiple low-weight operations between the data qubits and one or more ancilla qubits[69].

A key concept in QEC is that of the break-even point. A logical qubit containing n physical qubits has an error rate n times worse than a single physical qubit. Thus, every QEC code begins by

taking a giant step backward. It is up to the control system to find and correct the errors sufficiently rapidly and accurately that the rate of uncorrected logical qubit errors falls below that of the best single physical qubit comprising the logical qubit. The point at which the collective QEC process dynamics begins to actually increase the lifetime of the quantum information over the lifetime of the best of the individual components defines 'break even.'

A second key concept is fault tolerance, namely the reliable performance of QEC in the presence of imperfect ancillae and imperfect measurement and control operations. The task of fault-tolerant design is vastly more subtle and challenging than it is in traditional classical systems design. But, remarkably, with certain assumptions on the error model and the noise being below a certain threshold, quantum fault tolerance is in principle possible.

The goal of fault-tolerant system design is to prevent a 'chain reaction' of errors. This challenge can be met at the software level using 'transversal' gates[69] and more generally using error correction at intermediate steps of gates[70]. To prevent a blow up of the hardware parts count, it is also important to work below the software level, directly at the hardware level using, for example, 'error transparent' gates[52,71–75], 'biased-noise' qubits[76–81], and other techniques and qubit designs[24,82]. We are in the earliest stages of experiments exploring these techniques, and achieving robust and practical fault tolerance in large-scale systems remains a grand challenge for the entire field of quantum information processing. Meeting this remarkably difficult challenge will require achieving still lower natural qubit error rates, extremely high-fidelity multi-qubit gate operations and error syndrome measurements, all with minimal cross-talk.

Much industrial effort is currently being devoted towards the goal of realizing the surface code[58] within the circuit QED architecture[83–86]. This remarkable code uses a 2D lattice array of qubits that affords topological protection of the quantum information and requires only local weight-four error syndrome measurements. Only Clifford group operations can be directly implemented on the encoded states necessitating so-called magic-state injection to achieve universal control of individual logical qubits, something that is expected to require huge hardware overhead[87]. Recent theoretical advances in so-called lattice surgery techniques may prove useful in this regard[88–90].

Realistic theoretical simulations suggest that considerable further experimental progress will be required to reach the break-even point and will require as many as 49 physical qubits and a large complex of control and readout wiring[91]. This scale of hardware now exists[10] but has not yet demonstrated low enough error rates and weight-four error syndrome measurement with high enough fidelity for the surface code to reach break even.

It may be possible that this challenge can be met 'head on' through engineering, but at this early stage in the development of the field, an important intellectual challenge is to develop completely new ideas that will allow us to avoid the hardware count explosion and achieve practical fault tolerance in a manner that is much more hardware efficient.

Here again, circuit QED offers interesting perspectives. In the 'traditional' approach to circuit QED, the transmon anharmonic oscillators[18] are treated as discrete-variable (two-level) qubits (as in Fig. 4a), and the resonators are used as quantum buses[53] to couple the qubits via exchange of real and virtual photons.

A promising and radically different complementary approach is to use the microwave photon states of the resonators as logically encoded continuous variable ('bosonic') qubits (as in Fig. 4b) and use the anharmonic transmon oscillators as ancillae to provide universal control for the resonators[45,92]. This new approach has reached the break-even point[67] for quantum memory error correction and demonstrated a factor of two improvement in the fidelity of error-corrected gate operations on logically encoded qubits[74] in the presence of naturally occurring errors.
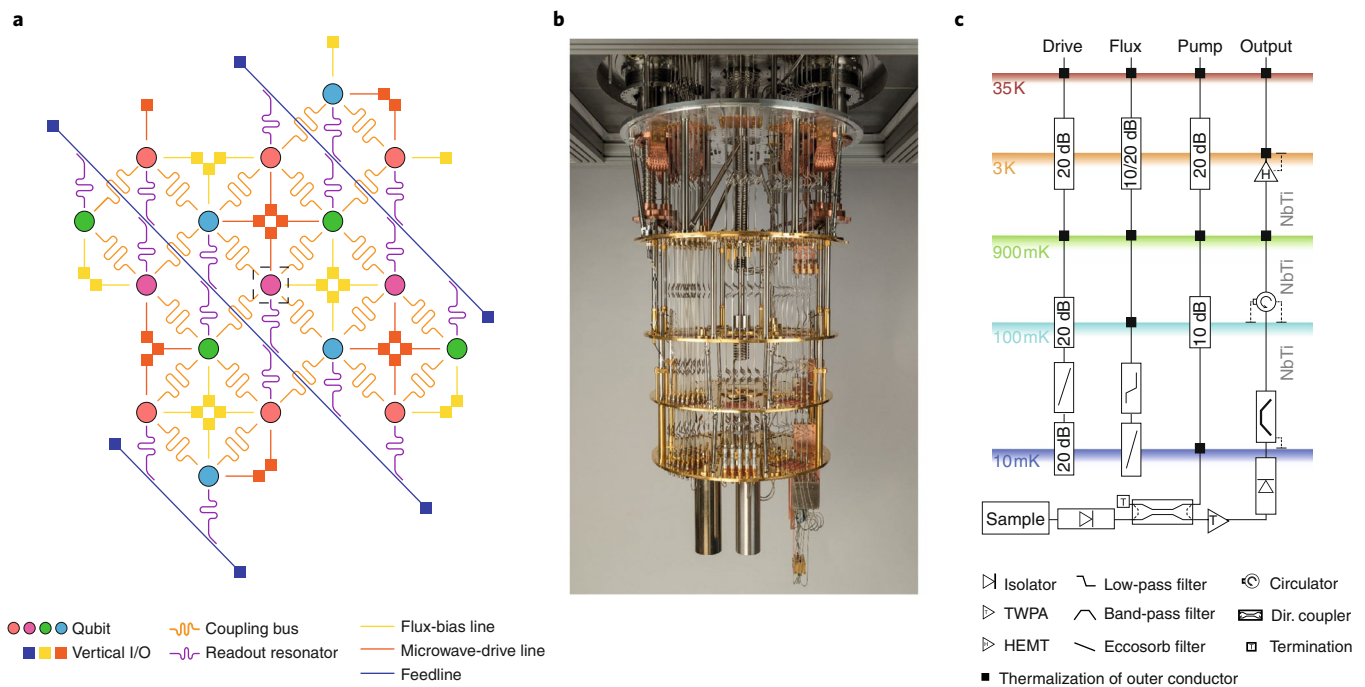
Fig. 5 | Quantum hardware. a, Electrical circuit schematic of a 17-qubit surface code, indicating the placement of the qubits and resonators used for qubit–qubit coupling and qubit readout. I/O stands for input/output. **b**, Dilution refrigerator used to cool superconducting chips through a series of stages spanning room temperature (top stage), 35 K, 3 K, 900 mK, 100 mK and 10 mK (bottom stage). Temperatures are approximate. The qubits are mounted inside electromagnetic shields (cylinders) below the 10 mK stage. Additional concentric thermal shields at each stage are not shown. Control and readout signals are conducted through the many coaxial wires running between temperature stages. **c**, Electrical schematic of control and readout infrastructure at the various temperatures stages used to control and readout qubits. TWPA, travelling-wave parametric amplifier; HEMT, high-electron-mobility transistor; Dir. coupler, directional coupler. Panels adapted with permission from: **a**, ref. [124], APS; **b,c**, ref. [110], Springer Nature Ltd.

In this regard, superconducting resonators have several advantages: they can easily have millisecond coherence times exceeding those of superconducting qubits by 10 to 20 times. Moreover, they bring the increased state space dimension needed for logical qubits by simply including more photons rather than increasing the number of physical qubits. Furthermore, the error model of microwave resonators is very simple and is dominated by photon loss (amplitude damping) with negligible dephasing.

A simple code exploiting these ideas and which corrects amplitude damping to the lowest order is the binomial code[93], for which QEC approaching the break-even point has also been recently demonstrated[68] using the logical states

$$|0_L\rangle = \frac{1}{\sqrt{2}}(|0\rangle + |4\rangle) \qquad (6)$$

$$|1_L\rangle = |2\rangle \qquad (7)$$

where $|n\rangle$ is the n-photon Fock state. This code was also used to achieve deterministic teleportation of an entangling gate on logically encoded states[94].

Because this code utilizes only a single bosonic mode, it requires the measurement of a single error syndrome to detect a photon loss error: the photon number parity. The parity of the photon number is a quantity that is very difficult to measure in ordinary quantum optics, but quite easy in circuit QED[67,95,96]. Because both logical states of the bosonic code are +1 eigenstates of parity, and both have the same mean photon number, the code satisfies the necessary conditions for lowest-order QEC[97]. Indeed, parity jumps tell us that a loss event occurred but nothing about the logical state in which it occurred.

This relative simplicity of the bosonic encoding is to be contrasted with the simplest qubit code for amplitude damping[98]. This code requires four qubits and measurement of three error syndromes to determine whether a decay error has occurred, and if so, on which of the four physical qubits it occurred. To first order in amplitude damping, this code has five possible error states, while the bosonic code has only two possible error states (loss of zero or one photon).

A further advantage of bosonic encoding is that the logical qubits stored as standing waves in a resonator can be released as travelling waves to achieve quantum communication and remote entanglement within the quantum computer (and beyond)[99,93,100]. The same error correctability that protects the logical bosonic qubits stored in resonators also protects them against errors in the communication process, so no additional encoding is required.

Because the resonator is a harmonic oscillator, classical drive tones cannot achieve universal quantum operations without the assistance of a nonlinear oscillator ancilla. Hence, the transmon is still needed, not as a qubit, but as a controller for the bosonic qubit. The controller coherence is not as good as that of the cavity it controls, but this is partially compensated by the fact that the controller idles much of the time since the error rate in the resonators is low. New ideas for 'hardware efficient' fault tolerance are being developed and demonstrated to further reduce the impact of controller errors without increasing the hardware overhead[52,71–75]. This line of research is bringing the field into the early stages of the era of fault-tolerant quantum computation.

Another exciting recent advance in continuous variable quantum information processing is the experimental realization of the states of the GKP[101] QEC code in trapped ions[102] and in circuit QED[46]. The code words consist of a periodic comb of squeezed states (or equivalently a uniform grid in phase space). Although originally
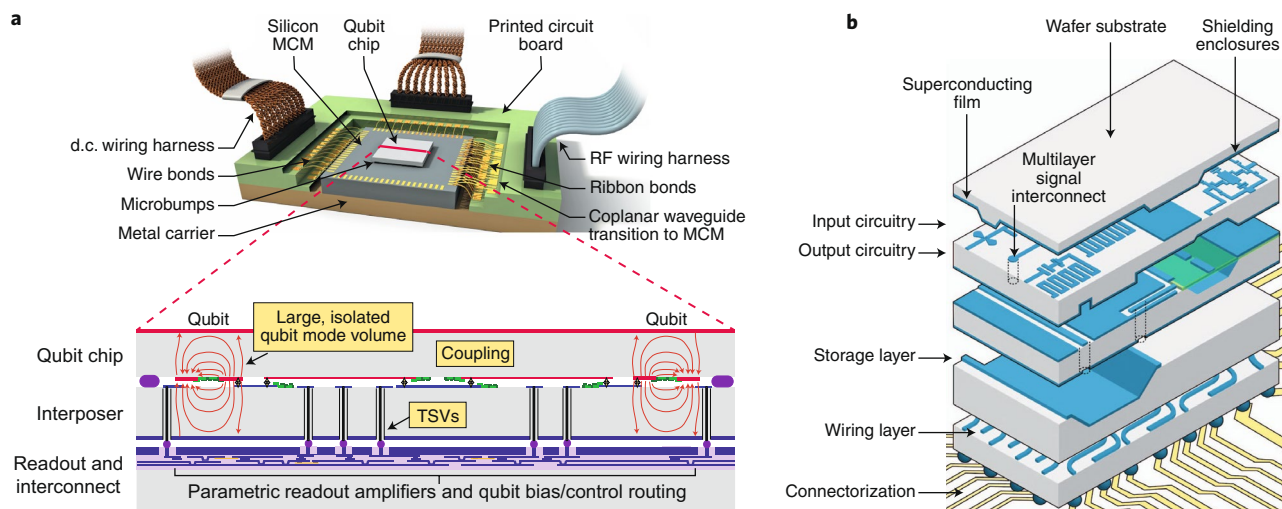
Fig. 6 | Three-dimensional integration of superconducting qubits. a, Three-tiered stack assembled from a qubit chip, interposer chip, and a multilayer readout and interconnect chip. Each chip is fabricated independently and then joined using thermocompression bump-bonding. MCM, multi-chip module; RF, radio frequency. **b**, Multilayer, micromachined cavities and apertures are assembled to form high-quality-factor resonators and host qubit chips used to mediate cavity control and readout. Panels adapted with permission from: **a**, ref. [113], Springer Nature Ltd; **b**, ref. [125], Springer Nature Ltd.

designed for mathematically simple but physically unrealistic oscillator displacement errors, this code has recently been shown to have excellent performance for physically realistic amplitude damping errors[103]. Simultaneous error correction for both logical bit- and phase-flip errors near the break-even point has also been demonstrated[46]. When originally proposed, the GKP code seemed to be far beyond the realm of experimental possibility, but the rapidly advancing capabilities in circuit QED now make this a very promising direction for near-term progress.

An interesting potential route for achieving fault tolerance is the design of qubits with highly biased noise channels (for example, qubits that have very few bit flips compared with phase flips). The same features of circuit QED mentioned above that permit observation of novel effects of squeezed light on superconducting qubits allow one to engineer a biased-noise cat qubit in cavities using two-photon driving and dissipation, and in transmon qubits using two-photon driving. These cat states suffer predominantly from only one type of error (associated with single-photon gain or loss) and are predicted to have a higher error threshold for fault tolerance[77–79] due to certain topological properties[78]. Preliminary experimental results are encouraging[80,81].

So far we have discussed error-correctable bosonic logical qubits stored in a single microwave resonator. We note that a 2D array of such resonators could be assembled to implement the surface code as a second level of QEC. This could be done with any of the existing bosonic codes (binomial[97], cat[67], GKP[46,101]) or even with the 'bare' unencoded states consisting simply of 0 and 1 photons. Because errors in the GKP code words correspond to continuous translations in phase space, decoding the errors in the second-level surface code has some interesting connections to gauge field theories[104].

The case of biased-noise qubits[77–81] would be especially interesting because recent theoretical work has demonstrated that a properly constructed surface code can have a very high error threshold (approaching 50% for the code capacity threshold and exceeding 5% for the fault-tolerance threshold) when constructed from an array of biased-noise qubits[105,106]. These results assume the existence of a bias-preserving controlled NOT gate, something that is not possible with ordinary two-level qubits, but has recently been proven to be possible with pumped cat qubits[78].

Practical challenges

Quantum information processing with circuit QED is rapidly transitioning from the realm of scientific curiosity to the threshold of technical reality[107]. Making this transition presents numerous practical challenges that stand squarely in the subject domain of quantum engineering, a developing new discipline that serves to bridge traditional quantum science and classical engineering in support of building extensible quantum machines[19]. Although the engineering abstractions associated with system scalability, for example, the quantum analogues of Dennard scaling or Moore's law, have yet to be developed for quantum information processors as they are yet still too immature, we can articulate the present challenges — as we understand them today — in extending current practice to larger-scale systems and applications (Fig. 5).

The generic needs of a quantum information processor can be summarized along the following lines. Quantum processors must be built from high-coherence materials using reproducible, extensible fabrication processes[108]. Once fabricated, they must be controlled and read out with high fidelity, a challenge that becomes more daunting as the number of qubits increases. There is both the need for the ingress and egress of larger numbers of control and readout signals to the processor, as well as a 'tyranny of interconnects' in routing those signals within the processor[109]. There is the need to calibrate the individual qubit and cavity frequencies, and their couplings to one another, to properly control and readout the processor, as well as to null out classical cross-talk and unwanted coherent Hamiltonian dynamics[54,85]. One must furthermore house and thermalize the processor — and all its control lines and, possibly, cryogenic electronics — in a manner consistent with its high-fidelity operation in a dilution refrigerator with limited heat-handling capacity at millikelvin temperatures[110]. And, one must develop a set of electronics and a software stack to implement the given algorithms at scale[111].

The challenges in meeting these needs are related in part to two distinct eras of scaling. The first is a nearer-term 'brute-force era', where each qubit is essentially individually wired for control and readout. Contemporary qubit processors with up to several tens of qubits fall in this category[10,112]. Such brute-force approaches are viable up to around 1,000 qubits — a loose estimate — limited primarily by packaging, signal routing and the size of dilution refrig-

erator one is willing to manufacture. The second may be referred to as the 'scaling era', where integrated methods — such as signal multiplexing and co-located, cryogenic electronics — are introduced to enable the control and readout of more qubits with fewer wires at the expense of higher complexity and heat load.

The two types of superconducting qubit circuits discussed here — planar circuit QED and microwave bosonic qubits — share many of these challenges, albeit to differing degrees. With the planar approach, the superconducting qubits themselves hold the quantum information and microwave cavities are used to read out the quantum states and, in some cases, mediate qubit coupling and control. Such planar processors benefit from semiconductor fabrication methods, including lithographic extensibility, manufacturability on silicon chips and relatively small form factors. The challenges reside in maintaining high coherence as the fabrication processes become more complex to meet the needs mentioned above. In the bosonic-qubit approach, relatively large (centimetre-scale) microwave cavities are machined in blocks of aluminium to hold the photonic quantum states, and the transmon qubits are used to control these states. The primary advantage of this approach is a degree of modularity and higher cavity-photon lifetimes, at the expense of a much larger footprint. As mentioned before, today, both approaches achieve approximately the same level of gate fidelity, around 99.9% for single-qubit gates and 99% for two-qubit gates[25].

Both the planar-qubit and cavity-photon approaches will rely on 3D integration to facilitate extensibility (Fig. 6). The bosonic-qubit approach is by its very nature 3D integrated, whereas the 2D planar-qubit approach leverages 3D integration technologies in a more conventional context[113]. As one moves from 1D chains of qubits[66,85] to larger 2D arrays, the signal routing to the inner qubits becomes practically prohibitive without utilizing the third dimension to enable interconnects to cross and bypass one another. Although one may envision fabrication of multiple wiring layers alongside qubits in a single monolithic process, such an approach generally incorporates lossy dielectrics between wiring layers and reduces qubit coherence. While monolithic fabrication with high-quality dielectrics may one day be a plausible and potentially advantageous approach for integrated qubit and control electronics, in the meantime, an alternative approach is to bump-bond together individual chips fabricated according to their respective functionality, for example, a qubit chip with high coherence, a multilayer interconnect chip for signal routing and a through-silicon-via (TSV) chip that connects them while isolating the highly sensitive qubit chip from the lossy dielectrics in the interconnect chip[113].

Although 3D integration helps address the 'tyranny of interconnects', it alone does not solve it. As the number of qubits increases, there is an increased demand on the number of signal lines that must be connected to the qubit package (housing). Today, those signals are generated using electronics at room temperature and brought into the dilution refrigerator along coaxial wiring that must be properly thermalized[110]. Advances include the use of flex cabling to reduce the heat load on the refrigerator and to increase the density of wiring. Bringing the control electronics into the refrigerator, for example, using cryogenic complementary metal–oxide–semiconductor (CMOS)[114] or superconducting single-flux-quantum (SFQ)[115] logic, serves to shorten the length of the signal wires, but it does not reduce the number of wires connecting to the package unless the cryogenic electronics are directly integrated with the qubits. In practice, cryogenic CMOS dissipates too much power to be viable in proximity to the qubits at the millikelvin stage of today's refrigerators. SFQ-based electronics or its derivatives may provide a solution, but is currently less mature than its CMOS counterpart. These problems may not be prohibitive in the brute-force era, but they will need to be addressed in the scaling era.

Outlook

Superconducting qubits and the circuit QED architecture have enabled tremendous experimental and theoretical advances over the past 15 years. With single-qubit and two-qubit gate fidelities currently standing at the 99–99.95% level, it is now possible to execute small-scale quantum algorithms with increasing circuit width (number of qubits) and depth (number of gates), including quantum simulations of small molecular systems[116,117], the dynamics of chemical physics processes[118] and quantum many-body simulations[119,120], as well as a recent report of the demonstration of quantum computational supremacy[10]. In addition, quantum networking using error correctable photonic codes is now being explored for use in distributed, modular computing architectures[99]. Beyond quantum computation, circuit QED techniques are now being applied to quantum-sensing applications in areas such as the search for dark matter[121,122].

Much work remains before quantum computers — even small-scale ones — become a practical reality. However, the circuit QED architecture provides an excellent platform for superconducting qubits to perform both the fundamental science and foundational engineering that will support the larger-scale systems of qubits needed to realize quantum algorithms of practical importance.

References

1. Haroche, S. & Raimond, J.-M. *Exploring the Quantum: Atoms, Cavities, and Photons* (Oxford Univ. Press, 2006).
2. Leibfried, D., Blatt, R., Monroe, C. & Wineland, D. Quantum dynamics of single trapped ions. *Rev. Mod. Phys.* **75**, 281–324 (2003).
3. Nakamura, Y., Pashkin, Y. & Tsai, J. Coherent control of macroscopic quantum states in a single-Cooper-pair box. *Nature* **398**, 786–788 (1999).
   This paper reports the observation of coherent quantum dynamics in superconducting quantum circuits.
4. Vion, D. et al. Manipulating the quantum state of an electrical circuit. *Science* **296**, 886–889 (2002).
5. Chiorescu, I., Nakamura, Y., Harmans, C. J. P. M. & Mooij, J. E. Coherent quantum dynamics of a superconducting flux qubit. *Science* **299**, 1869–1871 (2003).
6. Martinis, J. M., Devoret, M. H. & Clarke, J. Quantum Josephson junctions and the dawn of artificial atoms. *Nat. Phys.* https://doi.org/10.1038/s41567-020-0829-5 (2020).
7. Blais, A., Huang, R.-S., Wallraff, A., Girvin, S. M. & Schoelkopf, R. J. Cavity quantum electrodynamics for superconducting electrical circuits: an architecture for quantum computation. *Phys. Rev. A* **69**, 062320 (2004).
   This paper theoretically introduces the circuit QED architecture.
8. Wallraff, A. et al. Strong coupling of a single photon to a superconducting qubit using circuit quantum electrodynamics. *Nature* **431**, 162–167 (2004).
   This paper experimentally demonstrates circuit QED, in particular reporting the observation of vacuum Rabi splitting.
9. Haroche, S., Brune, M. & Raimond, J. M. From cavity to circuit quantum electrodynamics. *Nat. Phys.* https://doi.org/10.1038/s41567-020-0812-1 (2020).
10. Arute, F. et al. Quantum supremacy using a programmable superconducting processor. *Nature* **574**, 505–510 (2019).
    This paper reports 'quantum supremacy' with transmon qubits and circuit QED-based dispersive readout.
11. Pozar, D. M. *Microwave Engineering* (Wiley, 2012).
12. Vool, U. & Devoret, M. Introduction to quantum electromagnetic circuits. *Int. J. Circuit Theor. Appl.* **45**, 897–934 (2017).
13. Megrant, A. et al. Planar superconducting resonators with internal quality factors above one million. *Appl. Phys. Lett.* **100**, 113510 (2012).
14. Vissers, M. R., Kline, J. S., Gao, J., Wisbey, D. S. & Pappas, D. P. Reduced microwave loss in trenched superconducting coplanar waveguides. *Appl. Phys. Lett.* **100**, 082602 (2012).
15. Bruno, A. et al. Reducing intrinsic loss in superconducting resonators by surface treatment and deep etching of silicon substrates. *Appl. Phys. Lett.* **106**, 182601 (2015).
16. Calusine, G. et al. Analysis and mitigation of interface losses in trenched superconducting coplanar waveguide resonators. *Appl. Phys. Lett.* **112**, 062601 (2018).
17. Reagor, M. et al. Quantum memory with millisecond coherence in circuit QED. *Phys. Rev. B* **94**, 014506 (2016).

18. Koch, J. et al. Charge-insensitive qubit design derived from the Cooper pair box. *Phys. Rev. A* **76**, 042319 (2007).
19. Krantz, P. et al. A quantum engineer's guide to superconducting qubits. *Appl. Phys. Rev.* **6**, 021318 (2019).
20. Sheldon, S. et al. Characterizing errors on qubit operations via iterative randomized benchmarking. *Phys. Rev. A* **93**, 012301 (2016).
21. Orlando, T. P. et al. Superconducting persistent-current qubit. *Phys. Rev. B* **60**, 15398–15413 (1999).
22. Yan, F. et al. The flux qubit revisited to enhance coherence and reproducibility. *Nat. Commun.* **7**, 12964 (2016).
23. Manucharyan, V. E., Koch, J., Glazman, L. I. & Devoret, M. H. Fluxonium: single Cooper-pair circuit free of charge offsets. *Science* **326**, 113–116 (2009).
24. Gyenis, A. et al. Experimental realization of an intrinsically error-protected superconducting qubit. Preprint at https://arxiv.org/abs/1910.07542 (2019).
25. Kjaergaard, M. et al. Superconducting qubits: current state of play. Preprint at https://arxiv.org/abs/1905.13641 (2019).
26. Wendin, G. Quantum information processing with superconducting circuits: a review. *Rep. Prog. Phys.* **80**, 106001 (2017).
27. Bloch, F. & Siegert, A. Magnetic resonance for nonrotating fields. *Phys. Rev.* **57**, 522–527 (1940).
28. Devoret, M., Girvin, S. M. & Schoelkopf, R. J. Circuit-QED: How strong can the coupling between a Josephson junction atom and a transmission line resonator be? *Ann. Phys* **16**, 767–779 (2007).
29. Paik, H. et al. Observation of high coherence in Josephson junction qubits measured in a three-dimensional circuit QED architecture. *Phys. Rev. Lett.* **107**, 240501 (2011).
   This paper introduces the '3D transmon'.
30. Gu, X., Kockum, A. F., Miranowicz, A., Liu, Y.-x & Nori, F. Microwave photonics with superconducting quantum circuits. *Phys. Rep.* **718–719**, 1–102 (2017).
31. Thompson, R., Rempe, G. & Kimble, H. Observation of normal-mode splitting for an atom in an optical cavity. *Phys. Rev. Lett.* **68**, 1132–1135 (1992).
32. Boca, A. et al. Observation of the vacuum rabi spectrum for one trapped atom. *Phys. Rev. Lett.* **93**, 233603 (2004).
33. Maunz, P. et al. Normal-mode spectroscopy of a single-bound-atom–cavity system. *Phys. Rev. Lett.* **94**, 033002 (2005).
34. Gardiner, C. W. Inhibition of atomic phase decays by squeezed light: a direct effect of squeezing. *Phys. Rev. Lett.* **56**, 1917–1920 (1986).
35. Carmichael, H. J., Lane, A. S. & Walls, D. F. Resonance fluorescence from an atom in a squeezed vacuum. *Phys. Rev. Lett.* **58**, 2539–2542 (1987).
36. Carmichael, H. J. Viewpoint: squeezed light reengineers resonance fluorescence. *Physics* **9**, 77 (2016).
37. Turchette, Q. A., Georgiades, N. P., Hood, C. J., Kimble, H. J. & Parkins, A. S. Squeezed excitation in cavity QED: experiment and theory. *Phys. Rev. A* **58**, 4056–4077 (1998).
38. Castellanos-Beltran, M. A., Irwin, K. D., Hilton, G. C., Vale, L. R. & Lehnert, K. W. Amplification and squeezing of quantum noise with a tunable Josephson metamaterial. *Nat. Phys.* **4**, 929–931 (2008).
39. Murch, K. W., Weber, S. J., Beck, K. M., Ginossar, E. & Siddiqi, I. Suppression of the radiative decay of atomic coherence in squeezed vacuum. *Nature* **499**, 62–65 (2013).
40. Toyli, D. M. et al. Resonance fluorescence from an artificial atom in squeezed vacuum. *Phys. Rev. X* **6**, 031004 (2016).
41. Hofheinz, M. et al. Generation of Fock states in a superconducting quantum circuit. *Nature* **454**, 310–314 (2008).
42. Hofheinz, M. et al. Synthesizing arbitrary quantum states in a superconducting resonator. *Nature* **459**, 546–549 (2009).
43. Schuster, D. I. et al. Resolving photon number states in a superconducting circuit. *Nature* **445**, 515–518 (2007).
44. Khaneja, N., Reiss, T., Kehlet, C., Schulte-Herbruggen, T. & Glaser, S. J. Optimal control of coupled spin dynamics: design of NMR pulse sequences by gradient ascent algorithms. *J. Magn. Reson.* **172**, 296–305 (2005).
45. Heeres, R. W. et al. Implementing a universal gate set on a logical qubit encoded in an oscillator. *Nat. Commun.* **8**, 94 (2017).
46. Campagne-Ibarcq, P. et al. A stabilized logical quantum bit encoded in grid states of a superconducting cavity. Preprint at https://arxiv.org/abs/1907.12487 (2019).
47. Blais, A. et al. Quantum-information processing with circuit quantum electrodynamics. *Phys. Rev. A* **75**, 032329 (2007).
48. Wallraff, A. et al. Approaching unit visibility for control of a superconducting qubit with dispersive readout. *Phys. Rev. Lett.* **95**, 060501 (2005).
49. Clerk, A. A., Devoret, M. H., Girvin, S. M., Marquardt, F. & Schoelkopf, R. J. Introduction to quantum noise, measurement, and amplification. *Rev. Mod. Phys.* **82**, 1155–1208 (2010).
50. Walter, T. et al. Rapid high-fidelity single-shot dispersive readout of superconducting qubits. *Phys. Rev. Appl.* **7**, 054020 (2017).
51. Schuster, D. I. et al. ac Stark shift and dephasing of a superconducting qubit strongly coupled to a cavity field. *Phys. Rev. Lett.* **94**, 123602 (2005).
52. Elder, S. S. et al. High-fidelity measurement of qubits encoded in multilevel superconducting circuits. *Phys. Rev. X* **10**, 011001 (2020).
53. Majer, J. et al. Coupling superconducting qubits via a cavity bus. *Nature* **449**, 443–447 (2007).
54. Sheldon, S., Magesan, E., Chow, J. M. & Gambetta, J. M. Procedure for systematically tuning up cross-talk in the cross-resonance gate. *Phys. Rev. A* **93**, 060302 (2016).
55. Arute, F. et al. Quantum supremacy using a programmable superconducting processor. *Nature* **574**, 505–510 (2019).
56. Shor, P. W. Scheme for reducing decoherence in quantum computer memory. *Phys. Rev. A* **52**, R2493–R2496 (1995).
57. Steane, A. M. Error correcting codes in quantum theory. *Phys. Rev. Lett.* **77**, 793–797 (1996).
58. Kitaev, A. Y. Fault-tolerant computation by anyons. *Ann. Phys.* **303**, 2–30 (2003).
   This paper describes topologically protected logical qubits.
59. Cory, D. G. et al. Experimental quantum error correction. *Phys. Rev. Lett.* **81**, 2152–2155 (1998).
60. Knill, E., Laflamme, R., Martinez, R. & Negrevergne, C. Benchmarking quantum computers: the five-qubit error correcting code. *Phys. Rev. Lett.* **86**, 5811–5814 (2001).
61. Chiaverini, J. et al. Realization of quantum error correction. *Nature* **432**, 602–605 (2004).
62. Schindler, P. et al. Experimental repetitive quantum error correction. *Science* **332**, 1059–1061 (2011).
63. Waldherr, G. et al. Quantum error correction in a solid-state hybrid spin register. *Nature* **506**, 204–207 (2014).
64. Taminiau, T. H., Cramer, J., van der Sar, T., Dobrovitski, V. V. & Hanson, R. Universal control and error correction in multi-qubit spin registers in diamond. *Nat. Nanotechnol.* **9**, 171–176 (2014).
65. Reed, M. D. et al. Realization of three-qubit quantum error correction with superconducting circuits. *Nature* **482**, 382–385 (2012).
66. Kelly, J. et al. State preservation by repetitive error detection in a superconducting quantum circuit. *Nature* **519**, 66–69 (2015).
67. Ofek, N. et al. Extending the lifetime of a quantum bit with error correction in superconducting circuits. *Nature* **536**, 441–445 (2016).
   This paper reports QEC with a bosonic 'cat code' that reaches the break-even point.
68. Hu, L. et al. Quantum error correction and universal gate set operation on a binomial bosonic logical qubit. *Nat. Phys.* **15**, 503–508 (2019).
69. Nielsen, M. A. & Chuang, I. L. *Quantum Computation and Quantum Information* (Cambridge Univ. Press, 2010).
70. Yoder, T. J., Takagi, R. & Chuang, I. L. Universal fault-tolerant gates on concatenated stabilizer codes. *Phys. Rev. X* **6**, 031039 (2016).
71. Kapit, E. Error-transparent quantum gates for small logical qubit architectures. *Phys. Rev. Lett.* **120**, 050503 (2018).
72. Rosenblum, S. et al. Fault-tolerant detection of a quantum error. *Science* **361**, 266–270 (2018).
73. Hann, C. T. et al. Robust readout of bosonic qubits in the dispersive coupling regime. *Phys. Rev. A* **98**, 022305 (2018).
74. Reinhold, P. et al. Error-corrected gates on an encoded qubit. Preprint at https://arxiv.org/abs/1907.12327 (2019).
75. Ma, Y. et al. Error-transparent operations on a logical qubit protected by quantum error correction. Preprint at https://arxiv.org/abs/1909.06803 (2019).
76. Aliferis, P. & Preskill, J. Fault-tolerant quantum computation against biased noise. *Phys. Rev. A* **78**, 052331 (2008).
77. Puri, S. et al. Stabilized cat in a driven nonlinear cavity: a fault-tolerant error syndrome detector. *Phys. Rev. X* **9**, 041009 (2019).
78. Puri, S. et al. Bias-preserving gates with stabilized cat qubits. Preprint at https://arxiv.org/abs/1905.00450 (2019).
79. Guillaud, J. & Mirrahimi, M. Repetition cat-qubits: fault-tolerant quantum computation with highly reduced overhead. *Phys. Rev. X* **9**, 041053 (2019).
80. Grimm, A. et al. The Kerr-cat qubit: stabilization, readout, and gates. Preprint at https://arxiv.org/abs/1907.12131 (2019).
81. Lescanne, R. et al. Exponential suppression of bit-flips in a qubit encoded in an oscillator. Preprint at https://arxiv.org/abs/1907.11729 (2019).
82. Chao, R. & Reichardt, B. W. Fault-tolerant quantum computation with few qubits. *npj Quantum Inf.* **4**, 42 (2018).
83. Takita, M. et al. Demonstration of weight-four parity measurements in the surface code architecture. *Phys. Rev. Lett.* **117**, 210505 (2016).
84. Córcoles, A. D. et al. Demonstration of a quantum error detection code using a square lattice of four superconducting qubits. *Nat. Commun.* **6**, 6979 (2015).
85. Barends, R. et al. Superconducting quantum circuits at the surface code threshold for fault tolerance. *Nature* **508**, 500–503 (2014).
86. Versluis, R. et al. Scalable quantum circuit and control for a superconducting surface code. *Phys. Rev. Appl.* **8**, 034021 (2017).

87. Fowler, A. G., Mariantoni, M., Martinis, J. M. & Cleland, A. N. Surface codes: towards practical large-scale quantum computation. *Phys. Rev. A* **86**, 032324 (2012).
This paper is a pedagogical review of surface codes.
88. Litinski, D. & von Oppen, F. Quantum computing with Majorana fermion codes. *Phys. Rev. B* **97**, 205404 (2018).
89. Litinski, D. & von Oppen, F. Lattice surgery with a twist: simplifying clifford gates of surface codes. *Quantum* **2**, 62 (2018).
90. Litinski, D. A game of surface codes: large-scale quantum computing with lattice surgery. *Quantum* **3**, 128 (2019).
91. O'Brien, T. E., Tarasinski, B. & DiCarlo, L. Density-matrix simulation of small surface codes under current and projected experimental noise. *npj Quantum Inf.* **3**, 39 (2017).
92. Krastanov, S. et al. Universal control of an oscillator with dispersive coupling to a qubit. *Phys. Rev. A* **92**, 040303 (2015).
93. Axline, C. J. et al. On-demand quantum state transfer and entanglement between remote microwave cavity memories. *Nat. Phys.* **14**, 705–710 (2018).
94. Chou, K. S. et al. Deterministic teleportation of a quantum gate between two logical qubits. *Nature* **561**, 368–373 (2018).
95. Vlastakis, B. et al. Deterministically encoding quantum information using 100-photon Schrödinger cat states. *Science* **342**, 607–610 (2013).
96. Sun, L. et al. Tracking photon jumps with repeated quantum non-demolition parity measurements. *Nature* **511**, 444–448 (2014).
97. Michael, M. H. et al. New class of quantum error-correcting codes for a bosonic mode. *Phys. Rev. X* **6**, 031006 (2016).
This paper introduces the family of binomial error correction codes.
98. Leung, D. W., Nielsen, M. A., Chuang, I. L. & Yamamoto, Y. Approximate quantum error correction can lead to better codes. *Phys. Rev. A* **56**, 2567–2573 (1997).
99. Pfaff, W. et al. Controlled release of multiphoton quantum states from a microwave cavity memory. *Nat. Phys.* **13**, 882–887 (2017).
100. Muralidharan, S. et al. Optimal architectures for long distance quantum communication. *Sci. Rep.* **6**, 20463 (2016).
101. Gottesman, D., Kitaev, A. & Preskill, J. Encoding a qubit in an oscillator. *Phys. Rev. A* **64**, 012310 (2001).
This paper introduces the GKP 'grid' states for bosonic QEC.
102. Flühmann, C. et al. Encoding a qubit in a trapped-ion mechanical oscillator. *Nature* **566**, 513–517 (2019).
103. Albert, V. V. et al. Performance and structure of single-mode bosonic codes. *Phys. Rev. A* **97**, 032346 (2018).
104. Vuillot, C., Asasi, H., Wang, Y., Pryadko, L. P. & Terhal, B. M. Quantum error correction with the toric Gottesman-Kitaev-Preskill code. *Phys. Rev. A* **99**, 032344 (2019).
105. Tuckett, D. K. et al. Tailoring surface codes for highly biased noise. *Phys. Rev. X* **9**, 041031 (2019).
106. Tuckett, D. K., Bartlett, S. D., Flammia, S. T. & Brown, B. J. Fault-tolerant thresholds for the surface code in excess of 5% under biased noise. Preprint at https://arxiv.org/abs/1907.02554 (2019).
107. DiVincenzo, D. P. The physical implementation of quantum computation. *Fortschr. Phys*. **48**, 771–783 (2000).
This paper introduces the 'Divincenzo criteria' that any quantum computer must obey.
108. Oliver, W. D. & Welander, P. B. Materials in superconducting quantum bits. *MRS Bull.* **38**, 816–825 (2013).
109. Das, R. N. et al. Cryogenic qubit integration for quantum computing. In *Proc. IEEE 68th Electronic Components and Technology Conference (ECTC)* 504–514 (IEEE, 2018).
110. Krinner, S. et al. Engineering cryogenic setups for 100-qubit scale superconducting circuit systems. *EPJ Quantum Technol.* **6**, 2 (2019).
111. Jones, N. C. et al. Layered architecture for quantum computing. *Phys. Rev. X* **2**, 031007 (2012).
112. Corcoles, A. et al. Challenges and opportunities of near-term quantum computing systems. Preprint at https://arxiv.org/abs/1910.02894 (2019).
113. Rosenberg, D. et al. 3D integrated superconducting qubits. *npj Quantum Inf.* **3**, 42 (2017).
114. Barden, J. et al. A 28nm bulk-CMOS 4-to-8GHz <2mW cryogenic pulse modulator for scalable quantum computing. In *Proc. IEEE 2019 International Solid State Circuits Conference* 456–458 (IEEE, 2019).
115. Leonard, E. et al. Digital coherent control of a superconducting qubit. *Phys. Rev. Appl.* **11**, 014009 (2019).
116. Kandala, A. et al. Hardware-efficient variational quantum eigensolver for small molecules and quantum magnets. *Nature* **549**, 242–246 (2017).
117. O'Malley, P. J. J. et al. Scalable quantum simulation of molecular energies. *Phys. Rev. X* **6**, 031007 (2016).
118. Wang, C. S. et al. Quantum simulation of molecular vibronic spectra on a superconducting bosonic processor. Preprint at https://arxiv.org/abs/1908.03598 (2019).
119. Ma, R. et al. A dissipatively stabilized mott insulator of photons. *Nature* **566**, 51–57 (2019).
120. Chiaro, B. et al. Growth and preservation of entanglement in a many-body localized system. Preprint at https://arxiv.org/abs/1910.06024 (2019).
121. Zheng, H., Silveri, M., Brierley, R. T., Girvin, S. M. & Lehnert, K. W. Accelerating dark-matter axion searches with quantum measurement technology. Preprint at https://arxiv.org/abs/1607.02529 (2016).
122. Wang, Z. et al. Quantum microwave radiometry with a superconducting qubit. Preprint at https://arxiv.org/abs/1909.12295 (2019).
123. Fink, J. M. et al. Climbing the Jaynes–Cummings ladder and observing its nonlinearity in a cavity QED system. *Nature* **454**, 315–318 (2008).
124. Versluis, R. et al. Scalable quantum circuit and control for a superconducting surface code. *Phys. Rev. Appl.* **8**, 034021 (2017).
125. Brecht, T. et al. Multilayer microwave integrate quantum circuits for scalable quantum computing. *npj Quantum Inf.* **2**, 16002 (2016).

Acknowledgements

Author contributions

All authors contributed to the writing, editing and revision of the manuscript.

Competing interests

The authors declare no competing interests.

Additional information

Correspondence should be addressed to A.B.

Reprints and permissions information is available at www.nature.com/reprints.

Publisher's note Springer Nature remains neutral with regard to jurisdictional claims in published maps and institutional affiliations.